

STP 1645, 2023 / available online at www.astm.org / doi: 10.1520/STP164520220069

Pierre-Clément A. Simon,^{1,2} Long-Qing Chen,³ Mark R. Daymond,⁴
Arthur T. Motta,¹ and Michael R. Tonks⁵

Mechanisms of Mesoscale Hydride Morphology and Reorientation in a Polycrystal Investigated Using Phase-Field Modeling


Citation

P.-C. A. Simon, L.-Q. Chen, M. R. Daymond, A. T. Motta, and M. R. Tonks, "Mechanisms of Mesoscale Hydride Morphology and Reorientation in a Polycrystal Investigated Using Phase-Field Modeling," in *Zirconium in the Nuclear Industry: 20th International Symposium*, ed. S. K. Yagnik and M. Preuss (West Conshohocken, PA: ASTM International, 2023), 807–830, <http://doi.org/10.1520/STP164520220069>⁶

ABSTRACT


This study focuses on the precipitation of nanoscale hydrides in polycrystalline zirconium as a first step to predicting the hydride morphology observed experimentally and investigating the mechanisms responsible for hydride reorientation at the mesoscale. A quantitative phase-field model, which includes the elastic anisotropy of the nanoscale zirconium hydride system, is developed to


Manuscript received May 9, 2022; accepted for publication August 2, 2022.

¹Ken and Mary Alice Lindquist Department of Nuclear Engineering, 233 Hallowell Building, The Pennsylvania State University, University Park, PA 16802, USA P.-C. A. S.  <https://orcid.org/0000-0001-7083-2628>,

A. T. M.  <https://orcid.org/0000-0001-5735-1491>

²Computational Mechanics and Materials Department, Idaho National Laboratory, Idaho Falls, ID 83415, USA

³Department of Materials Science and Engineering, The Pennsylvania State University, University Park, PA 16802, USA  <https://orcid.org/0000-0003-3359-3781>

⁴Dept. of Mechanical and Materials Engineering, Queen's University, Kingston, ON K7L 2N8, Canada  <https://orcid.org/0000-0001-6242-7489>

⁵Dept. of Materials Science and Engineering, University of Florida, Gainesville, FL 32611, USA

 <https://orcid.org/0000-0002-1343-3193>

⁶ASTM 20th International Symposium on *Zirconium in the Nuclear Industry* held on June 20–23, 2022 in Ottawa, ON, Canada.

Copyright © 2023 by ASTM International, 100 Barr Harbor Drive, PO Box C700, West Conshohocken, PA 19428-2959.

ASTM International is not responsible, as a body, for the statements and opinions expressed in this paper. ASTM International does not endorse any products represented in this paper.

investigate the mechanism of hydride reorientation in which the presence of an applied hoop stress promotes hydride precipitation in grains with basal poles aligned with the circumferential direction. Although still elongated along the basal plane of the hexagonal matrix, nanoscale hydrides growing in grains oriented perpendicular to the applied stress appear radial at the mesoscale. Thus, a preferential hydride precipitation in grains with basal poles aligned parallel to the applied stress could account for mesoscale hydride reorientation. This mechanism is consistent with experimental observations performed in other studies.

Keywords

hydride reorientation, zirconium hydrides, phase-field modeling, experimental comparison, nuclear materials, polycrystal, microstructure evolution

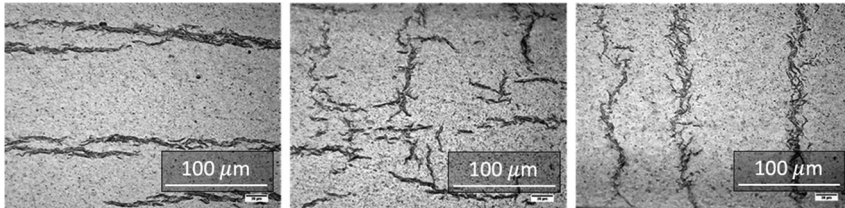
Introduction

The zirconium-based fuel cladding materials in light water reactors offer good high-temperature corrosion resistance in water, a low thermal neutron absorption cross section, good thermal conductivity, good resistance to void swelling and radiation damage, and adequate mechanical properties.¹ However, during normal operation, waterside corrosion occurs and hydrogen is created as a byproduct. A fraction of this hydrogen can be picked up by the cladding and precipitate into brittle hydrides once the hydrogen concentration reaches the solubility limit of the material.^{2–6} This can embrittle the zirconium alloy cladding depending on hydride orientation and morphology in the cladding.^{1,7} Whereas mesoscale hydrides tend to orient circumferentially in a zirconium cladding tube, the presence of an external tensile stress applied in the circumferential direction can lead to mesoscale hydride structures with an overall radial orientation, as shown in [figure 1](#). Previous experimental studies have quantified the stress needed to observe hydride reorientation (the threshold stress) and reported values between 50 and 220 MPa.^{1,8–12} However, despite extensive efforts to understand zirconium hydride morphology and reorientation, the mechanisms governing mesoscale hydride microstructure are still unknown.

Because of its versatility and powerful computational abilities, phase-field modeling is recognized as a valuable tool for studying microstructure evolution at the mesoscale^{13,14} and has been used to study hydride precipitation.^{1,15,16} Several studies have focused on the development of a quantitative phase-field model for the α -Zr/ δ -ZrH_{1.66} system in an attempt to explain hydride morphology with and without applied stress.^{17–23} However, the calculated threshold stress for reorientation was predicted by some models to be between 1.5 and 2.5 GPa,^{19,20,23} which is much higher than experimental measurements.

To improve predictions, several recent studies consider nanoscale hydrides stacking.^{17,21,22} Hydride particles are modeled as a multiscale structure, where nanoscale hydrides of a few dozen nanometers aggregate to form long mesoscale hydrides, as seen in [figure 1](#).^{1,8,24} Although models from Heo et al.²¹ and Han et al.²²

FIG. 1 Zirconium hydride micrograph from Cinbiz et al.⁸ showing circumferential hydrides obtained without applied stress (left), mixed hydrides obtained after one cycle under an applied stress of 150 MPa (center), and radial hydrides obtained after several cycles under an applied stress of 150 MPa (right). The multiscale hydride structure is visible.



predict the circumferential stacking of nanoscale hydrides under no applied stress, they describe reorientation as a continuous process. Mesoscale hydride orientation is predicted to progressively change from circumferential to radial as the magnitude of the applied stress increases. This contradicts experimental observations of hydride reorientation, where mesoscale hydrides are oriented either circumferentially, radially, or a mix of the two (see [fig. 1](#) and Motta et al.,¹ Cinbiz et al.,⁸ and Colas et al.⁹). Moreover, the existence of the large shear strain introduced in the elastic description of the α -Zr/ δ -ZrH_{1.66} system in these studies is still under debate.^{17,25,26}

Simon et al.¹⁷ successfully predicted the nanoscale hydride elongated shape, orientation, and stacking along the basal plane of the hexagonal zirconium matrix experimentally observed using transmission electron microscopy and scanning electron microscopy in the absence of applied stress. However, this model still fails to generate hydride reorientation at the mesoscale under reasonable applied stresses.^{17,27} This is attributed to the fact that the model was applied only to single-crystal α -Zr. In zirconium cladding materials, grain sizes range from a few to tens of microns,^{27,28} which means that nanoscale hydrides stack across hundreds of grains to form the mesoscale hydrides shown in [figure 1](#).⁸ Simulating hydride precipitation in a single grain corresponds to assuming infinitely large grains, and because reorientation is more difficult in a material with larger grains,^{27,29} it suggests that the mechanism for reorientation involves the grain structure.

The aim of the current study is to expand the quantitative phase-field model from Simon et al.¹⁷ to explore the effect of the zirconium crystal structure and texture on hydrogen distribution and hydride morphology with and without applied stress. In this paper, we summarize the phase-field model used, focus on the effect of the crystal structure of the zirconium cladding material on hydrogen distribution, and then turn our attention to hydride growth in polycrystals. These results and their significance are discussed before the paper is concluded.

Phase-Field Modeling of Hydrides in Polycrystalline Zirconium

As in Simon et al.,¹⁷ the phase-field model of the α -Zr/ δ -ZrH_{1.66} system uses the approach developed by Kim, Kim, and Suzuki (KKS) because of its versatility.³⁰ The decoupling of the interfacial width and energy reduces the computational costs.^{30,31} Moreover, the ability of the KKS approach to include the impact of lattice strain on hydrogen diffusion, which is a critical mechanism on the behavior of hydrogen in a zirconium grain structure, makes it a better choice than the grand potential model.³² In this section, we summarize the changes made to the model from Simon et al.¹⁷ to account for the crystal structure of the zirconium material.

PHASE-FIELD MODEL OF ZIRCONIUM HYDRIDE

The phase-field model described in detail in Simon et al.¹⁷ balances the chemical, interfacial, and elastic energy of the α -Zr/ δ -ZrH_{1.66} system to determine the equilibrium hydride microstructure. The variables c_α and c_δ describe the hydrogen atomic fraction in the α -Zr and δ -ZrH_{1.66} phases, respectively, and η is a continuous order parameter equal to 1 in δ -ZrH_{1.66} and to 0 in α -Zr. The equations governing microstructure evolution are the same in this study as in Simon et al.¹⁷ Note that, for reasons detailed below, the current model accounts for only one δ -hydride variant, even though Simon et al.¹⁷ included two. The chemical free energy f_{chem} of the system is defined as a parabolic approximation of the CALPHAD free energies of the α -Zr/ δ -ZrH_{1.66} system, which has been shown to accurately predict hydrogen concentration in both phases at equilibrium.^{17,18} f_{chem} is equal to

$$f_{chem}(c_\alpha, c_\delta, \eta) = h_\alpha(\eta)f_{chem}^\alpha(c_\alpha) + h_\delta(\eta)f_{chem}^\delta(c_\delta) \quad (1)$$

with h_α and h_δ interpolation functions defined in Simon et al.¹⁷ and Moelans³³ and

$$f_{chem}^v(c_v) = \frac{1}{2}\lambda_v(c_v - c_v^v)^2 + f_v^0 \quad (2)$$

with λ_v , c_v^v , and f_v^0 already defined in Simon et al.¹⁷ As in previous studies, the interfacial energy in the system is assumed to be isotropic and equal to 1.2483 eV/nm².^{17,21} The elastic energy f_{el} is derived using Khachaturyan's microelasticity theory, which provides the basis for a strain interpolation scheme:³⁴

$$f_{el} = \frac{1}{2}C_{ijkl}\epsilon_{ij}^{el}\epsilon_{kl}^{el} \quad (3)$$

where:

C_{ijkl} = interpolated stiffness tensor and
 ϵ_{ij}^{el} = elastic strain.¹⁷

As in Simon et al.,¹⁷ f_{el} accounts for the anisotropic elastic tensors of both α -Zr and δ -ZrH_{1.66}, the anisotropic stress-free strains due to the volume difference and shape change between the α -Zr phase and the δ -ZrH_{1.66} phase,^{17,35} the internal strain due

to the presence of hydrogen atoms in solid solution in the hexagonal zirconium matrix,³⁶ and the strain due to the anisotropic thermal expansion of the two phases.^{37,38} The elastic description of the system accounts for the crystallographic orientation of the fcc δ -ZrH_{1.66} phase in the hcp α -Zr phase and leverages experimental measurements and density functional theory calculations of stress-free strain and elastic tensor values. Note that the elastic interaction $f_{el}^{int,\delta}$, which is used to investigate the interaction between hydride particles with the matrix, is defined as in Simon et al.¹⁷:

$$f_{el}^{int,\delta} = \sigma_{ij} \left(\epsilon_{ij,\delta}^* - \epsilon_{ij,\alpha}^* \right) \quad (4)$$

where:

σ_{ij} = stress field and

$\epsilon_{ij,\alpha}^*$ and $\epsilon_{ij,\delta}^*$ = stress-free strains of the α -Zr and δ -ZrH_{1.66} phases listed above.

The model's parameters used in the current study, including chemical and elastic properties and kinetics parameters, are the same as the ones defined in Simon et al.¹⁷ The current phase-field model differs by introducing the zirconium polycrystalline structure, which is covered in detail in the next section.

INTRODUCTION OF THE ZIRCONIUM GRAIN STRUCTURE

In the phase-field model, the grain structure of the α -Zr phase is represented by the order parameter $\eta_{GB,i}$.³⁹ A given order parameter is equal to 1 in one grain and to 0 in neighboring grains, with the continuous transition from 1 to 0 occurring at the grain boundary (GB). To describe the GB, another continuous variable is defined as

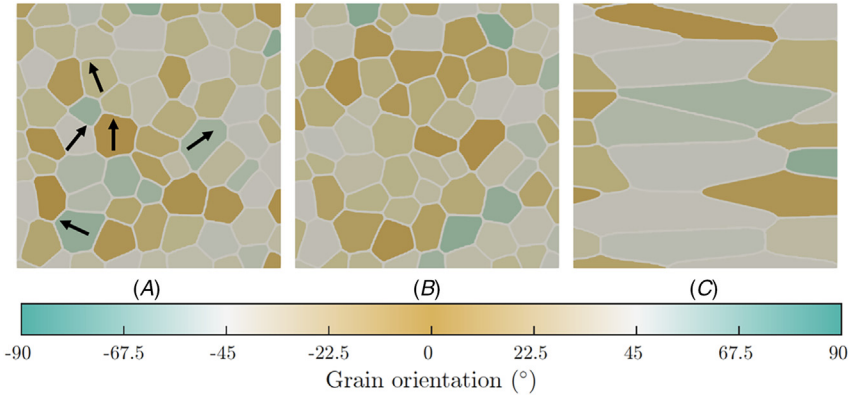
$$\chi = \sum_i \eta_{Gr,i}^2 \quad (5)$$

χ is equal to 1 in the grain interior and transitions continuously to 0.5 along the midplane of the GBs. Importantly, the α -Zr grain structure does not evolve in this phase-field model. Hydride precipitation occurs on a shorter time scale and at a different temperature than zirconium grain growth,^{1,40} so the zirconium grain structure remains immobile during hydride precipitation.

Generation of Zirconium Polycrystals

A method based on the approach described in Section 2.4.5.1 of Simon⁴⁰ was used to generate zirconium polycrystals with desired grain sizes, grain aspect ratios, GB widths, and crystallographic texture (described by Euler angles). **Figure 2** shows the 2D polycrystals created using this method, with GB widths of 4 nm and the desired texture described by the Kearns factor in the normal direction. The texture corresponds to cladding materials. However, the average grain sizes of the generated structures are significantly smaller than the 1- μ m average grain size of the experimental materials to include a reasonable number of grains without prohibitive computational costs. Because Kearns and Woods²⁷ showed that hydrides are more susceptible to reorient in a material with smaller grains, modeling a larger number

FIG. 2 Generated zirconium polycrystal structures colored to show grain orientation (i.e., the angle between the basal pole and radial (vertical) direction). (A, B) Same polycrystal but with different grain orientations. This polycrystal has equiaxed grains with an average diameter of 50 nm and a Kearns factor equal to 0.5826. (C) Polycrystal with elongated grains with an aspect ratio of 5, an average height of 50 nm, and a Kearns factor equal to 0.5744. The c vector ($[0001]_a$) of a few grains are added in (A) for clarity. The domain size is 400×400 nm.



of smaller grains might better enable an investigation of reorientation mechanisms than modeling a few large grains would. The script used to generate these polycrystals is available in Simon et al.^{41,42}

Segregation Energy at the Grain Boundary

Because GBs attract hydrogen in solid solution,^{1,43} the chemical description of the α -Zr phase is modified locally at GBs to make it more favorable for hydrogen atoms to aggregate there. At GBs, the minimum of the parabolic expression of the α -Zr chemical free energy density introduced in Simon et al.¹⁷ is slightly increased for the GB to accommodate more hydrogen. At the GB, the chemical free energy density is thus changed from equation (2) to

$$f_{chem}^{\alpha,GB}(c_\alpha) = \frac{1}{2}\lambda_\alpha(c_\alpha - c_\alpha^v - \Delta c_{GB}^v)^2 + f_\alpha^0 \quad (6)$$

where:

Δc_{GB}^v = shift in the concentration at the minimum of the chemical free energy parabola.

The chemical free energy density of the α -Zr is interpolated from the interior of the grains to the GB, leading to

$$f_{chem}^{\alpha,global} = (1 - h_{GB})f_{chem}^\alpha + h_{GB}f_{chem}^{\alpha,GB} \quad (7)$$

replacing f_{chem}^α in [equation \(1\)](#), with h_{GB} defined as

$$h_{GB}(\chi) = 1 - \frac{1}{2} \left(1 + \tanh \left(\frac{\chi - \chi_{\frac{1}{2}}}{d \sqrt{2}} \right) \right) \quad (8)$$

where:

$\chi_{\frac{1}{2}} = 0.75$ is the middle of the interface and
 $d = 0.06$ is the interface thickness.

The interpolation function in [equation \(8\)](#) is equal to 1 at the GB and to 0 within grains.

The appropriate concentration shift Δc_{GB}^v in the model introduces the correct segregation energy. To the authors' knowledge, the only estimation of the GB segregation energy for the hydrogen in zirconium is found in Christensen et al.⁴³ Using density functional theory, Christensen et al. derived the segregation energy of the Zr(0001)/Zr(0001) $\Sigma 7$ twist GB, defined as

$$E_{seg}^{GB} = (E_H^{GB} - E^{GB}) - (E_H^{bulk} - E^{bulk}) \quad (9)$$

where:

E^{bulk} = total energy of a pure bulk zirconium model,
 E_H^{bulk} = energy of a bulk model with hydrogen,
 E^{GB} = pure GB energy, and
 E_H^{GB} = GB energy containing hydrogen.

Because $E_H^{GB} - E^{GB} = f_{chem}^{\alpha, GB}(c_{\alpha, GB}^v) - f_{chem}^{\alpha, GB}(0)$, $E_H^{bulk} - E^{bulk} = f_{chem}^\alpha(c_\alpha^v) - f_{chem}^\alpha(0)$, and $f_{chem}^\alpha(c_\alpha^v) = f_{chem}^{\alpha, GB}(c_{\alpha, GB}^v)$, the segregation energy can be written as

$$E_{seg}^{GB} = f_{chem}^\alpha(0) - f_{chem}^{\alpha, GB}(0) \quad (10)$$

Injecting [equations \(2\)](#) and [\(7\)](#) into [equation \(10\)](#) and solving for Δc_{GB}^v provides

$$\Delta c_{GB}^v = -c_\alpha^v + \sqrt{c_\alpha^{v2} - 2 \frac{E_{seg}^{GB}}{\lambda_\alpha}} \quad (11)$$

which is equal to $\Delta c_{GB}^v = 2.49 \times 10^{-4} = \frac{1}{203} c_\alpha^v$ atomic fraction at $T = 550$ K with $E_{seg}^{GB} = -7.4$ eV/nm³ from Christensen et al.⁴³ Due to the limited data available, the segregation energy in all zirconium GBs is assumed to be equal to the value provided in Christensen et al.⁴³

Effect on Elastic Properties

To represent the grain texture, the stiffness tensors and the eigenstrains of the α -Zr and δ -ZrH_{1.66} phases are rotated from one grain to the next using the Euler angles. The stiffness tensors and the eigenstrains are interpolated across GBs using

$$h_i^{el}(\eta_{Gr,i}) = \frac{1}{2} (1 + \sin((\eta_{Gr,i} - 0.5)\pi)) \quad (12)$$

NUMERICAL METHOD

Our phase-field model is implemented using the Multiphysics Object-Oriented Simulation Environment, or MOOSE.^{44–47} Simulations are performed at $T = 550$ K to correspond to the early stages of hydride precipitation with a total concentration of hydrogen equal to $c_{tot} = 250$ or 350 wt.ppm. Hydride nuclei are introduced in the domain at $t = 0$ s as circular particles with a radius of 5 nm and with a hydrogen atomic fraction of 0.60 . The remaining hydrogen is uniformly distributed in the rest of the domain.

The size of the domain is limited by the computational cost of the simulations. The domain size varies depending on the simulation and is specified for each result. Because the interfacial thickness is fixed at 2 nm to resolve the smallest features of the domain, the cartesian mesh is defined with four or more levels of mesh adaptivity so that a minimum of five nodes are present across the interface. The time step size starts at 2×10^{-4} ms, and an adaptative time stepper readjusts the time step throughout the simulations to as high as 0.1 ms. These parameters were determined based on convergence studies to make sure that these parameters were fine enough to minimally affect the phase-field model predictions but coarse enough to limit computational costs.

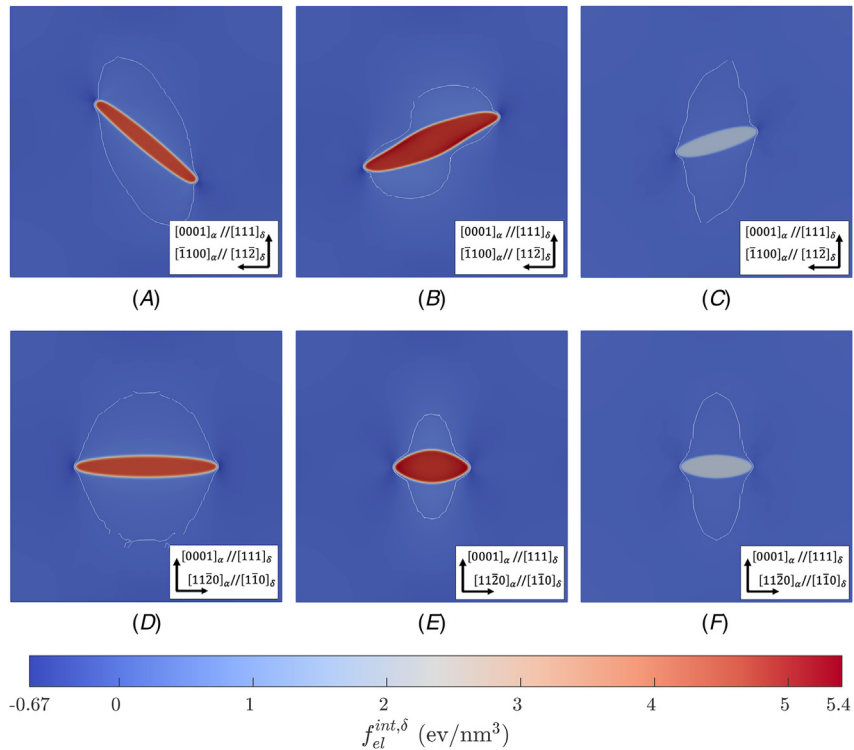
A zero-flux condition is imposed at the boundary for the variables c and η to isolate hydrogen and growing hydrides. The boundary conditions are defined to prevent rigid-body motion of the domain while limiting their effect on the stress field generated by the hydride. A plane strain condition is applied to the 2D simulation to assume that the thickness of the domain is comparable to its other dimensions. To study hydride growth under stress, an uniaxial applied stress of 250 MPa is introduced by applying a pressure on the desired edges of the domain.

JUSTIFICATION FOR 2D SIMULATIONS

To accurately represent the grain elongation and zirconium texture, it is important to include several dozens of grains within the simulation domains. Simulations in this study are performed in 2D domains to reduce computational costs while incorporating a significant number of grains into simulations. Although Simon et al.¹⁷ showed that the nanoscale hydrides have an inherently 3D shape, a carefully selected planar domain may provide a reasonable 2D approximation of hydride shape.

Figure 3 compares predictions from 2D simulations in the $(11\bar{2}0)_\alpha$ and $(\bar{1}100)_\alpha$ planes with 2D slices from 3D simulations presented in Simon et al.¹⁷ In the $(11\bar{2}0)_\alpha$ plane, the hydride predicted by the 2D simulation (**fig. 3C**) is oriented in a similar way as the hydride shown in **figure 3B**. In the $(\bar{1}100)_\alpha$ plane, the hydride predicted by the 2D simulation (**fig. 3F**) is elongated along the basal plane, as in the 3D simulations. In both planes, the top and bottom of the hydride are in compression, and the zones near the hydride edge are in tension, as predicted by the 3D simulations. 2D simulations predict a smaller hydride. This is because although both 2D and 3D simulations have a hydrogen composition of 250 wt.ppm, it corresponds to different total hydrogen amounts in a 2D or 3D domain, which results in

FIG. 3 Comparison of hydride morphology in the $(1\bar{1}20)_x$ (A–C) and $(\bar{1}100)_x$ (D–F) planes as determined by 3D and 2D simulations. (A), (D), (B), and (E) correspond to 2D slices of the results presented in figure 7 from Simon et al.¹⁷ (A), (D), (B), and (E) each show one of the two hydride shapes predicted in Simon et al.¹⁷ (C) and (F) are the results of 2D simulations at $t = 1.5$ ms. The domain size for the 2D simulations is 100×100 nm to correspond to the 3D simulations from Simon et al.¹⁷ The images are shaded by the elastic interaction energy $f_{el}^{int,\delta}$, with the contour for $f_{el}^{int,\delta} = 0$ in white. 2D simulations appropriately represent the hydride shape in specific planes.



different particle sizes at equilibrium. The difference in magnitude of the elastic interaction energy $f_{el}^{int,\delta}$ is attributed to the plane strain assumption used for the 2D simulation. The absence of eigenstrain in the third direction naturally decreases $f_{el}^{int,\delta}$. Although there are noticeable differences between the 2D and 3D simulations, as shown in figure 3, they are not expected to significantly affect hydride morphology. The most important features for hydride morphology and interaction (i.e., hydride shape, orientation, and the shape of the elastic interaction energy field around the hydride) are captured in the 2D simulations. 2D simulations can thus appropriately represent the hydride shape while reducing computational costs.

In the rest of this study, simulations are performed in the $(\bar{1}100)_\alpha$ plane. It is important to note that two δ -hydride variants were introduced in Simon et al.¹⁷ to represent the two different arrangements respecting the orientation relationship between the fcc δ -ZrH and hexagonal α -Zr structures. Although crucial in 3D simulations to accurately capture hydride particle interactions,¹⁷ they become equivalent in 2D simulations in the $(\bar{1}100)_\alpha$ plane because they both align with the α -Zr basal plane. For that reason, only one hydride variant is included in the current study.

Hydrogen Distribution in a Polycrystal

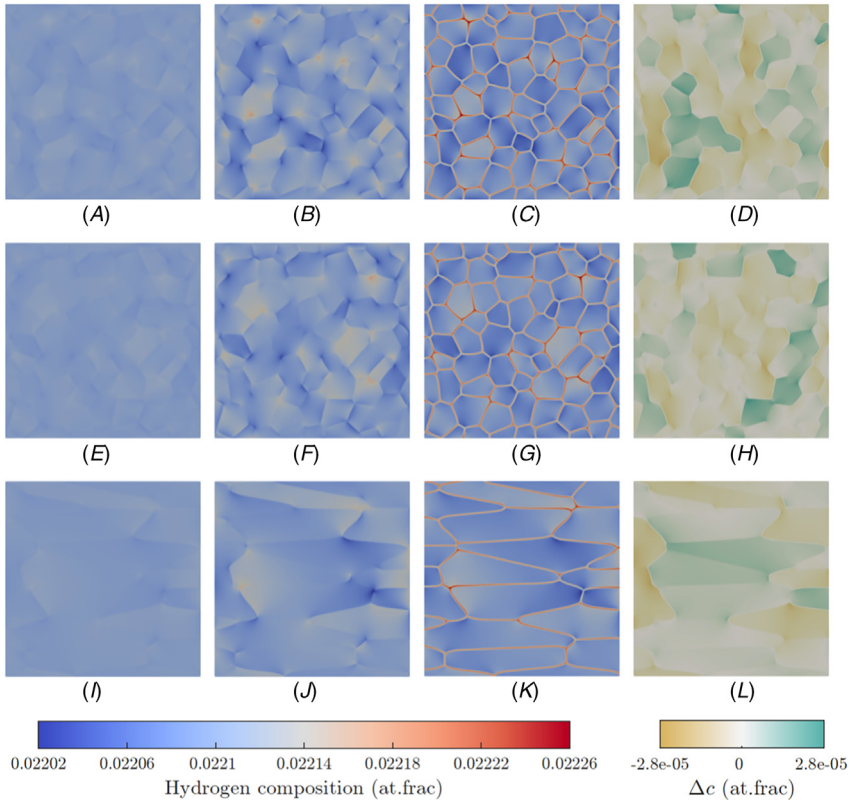
First, we study the effect of elastic anisotropy, segregation energy, and an applied stress of 250 MPa on hydrogen distribution in a polycrystal at $T = 550$ K without considering hydride precipitation. A uniform distribution of 250 wt.ppm is introduced in a polycrystal structure. Simulations were performed with and without thermal strains, segregation energy at the GB, and applied stress to identify the effect of each physics on hydrogen distribution. The polycrystals presented above were used to study the effect of grain shape, grain size, and texture on hydrogen distribution.

Figure 4 shows the results of these simulations. Figure 4A, E, and I shows that even without thermal strains, segregation energy, or applied load, the hydrogen distribution is not perfectly homogeneous. Because, as described previously, the model accounts, among other sources of strain, for the anisotropic strain due to the presence of hydrogen in solid solution in zirconium,¹⁷ their presence leads to an anisotropic expansion of the misoriented zirconium grains. This leads to heterogeneities in the stress field. Certain zones of the domain are under greater compression than others and can thus accommodate fewer hydrogen atoms, leading to a heterogeneous hydrogen distribution.

However, at $T = 550$ K and $c_{tot} = 250$ wt.ppm, this departure from a homogeneous hydrogen distribution is minor compared with the one due to the presence of thermal strains, as illustrated in figure 4B, F, and J. Like the strains due to the presence of hydrogen atoms, thermal strains are larger in the c direction of the hexagonal α -Zr crystal than in the basal plane. As a result, thermal strains lead to similar heterogeneities in the stress field and hydrogen distribution. Some GBs and triple junctions can be hydrogen-rich or hydrogen-deprived, depending on the relative orientation between the neighboring grains.

Adding the segregation energy at GBs introduced in equations 6–11 promotes the diffusion of hydrogen toward GBs, as shown in figure 4C, G, and K. However, the concentration of hydrogen is not uniform in all GBs. When the model includes both anisotropic thermal strains and the segregation energy, the two physical phenomena compete to influence hydrogen distribution. On the one hand, hydrogen tends to aggregate in GBs to minimize the chemical energy of the system; on the other hand, hydrogen diffuses toward grains, GBs, and triple junctions that are in more tension than other areas to minimize the elastic energy of the system. The hydrogen distribution presented in figure 4C, G, and K suggests that hydrides

FIG. 4 Hydrogen distribution with an average composition of 250 wt.ppm at 550 K in polycrystals from **figure 2** in atomic fraction without thermal strains or segregation (*A, E, I*), with thermal strains but no segregation (*B, F, J*), and with thermal strains and segregation (*C, G, K*). A 250-MPa applied load is only applied in (*D*), (*H*), and (*L*), which show the changes in hydrogen composition Δc from (*C*), (*G*), and (*K*) under a circumferential (horizontal) load. Thermal strains, segregation energy, and applied stress all contribute to a heterogeneous hydrogen distribution. The domain size is 400×400 nm.



are more likely to nucleate and grow at GBs and triple junctions in tension. This preference is consistent with experimental observations.^{24,48} Other defects not considered in this model, such as dislocations or other precipitates, could also locally influence hydrogen distribution. However, the mechanisms explained here are expected to remain valid.

When considering the effect of applied stress, it is important to realize that a polycrystalline material reacts differently to applied stress than a single crystal. In a single-crystal simulation, the basal pole of the hexagonal matrix is commonly assumed to correspond to the radial direction of the cladding because the material

is heavily textured with basal poles in the radial direction. The hoop stress is thus applied perpendicularly to the basal pole (i.e., circumferentially). In a polycrystal material, however, not all basal poles align perpendicularly to the circumferential direction. In this work, we consider that grains are misaligned with the direction of the applied load when their basal pole is not radial. The most misaligned grains would have their basal pole parallel to the direction of the applied stress (i.e., in the circumferential direction). When external stress is applied, misaligned grains and GBs react differently, thus changing the stress field and further influencing hydrogen distribution. **Figure 4D, H, and L** shows the effect of a circumferentially applied load on hydrogen distribution. These changes in hydrogen concentration correlate with grain orientation, as shown by comparing the polycrystals and textures shown in **figure 2** with the predictions shown in **figure 4D, H, and L**. Due to the elastic anisotropy, hydrogen tends to diffuse from aligned grains to misaligned grains. Even if these changes represent only a few wt.ppm in hydrogen content, it could be sufficient to lead to a higher probability of hydride nucleation in misaligned grains and in radially oriented GBs. Nanoscale hydrides nucleating in misaligned grains would then grow radially in the cladding while still respecting the orientation relationship with the α -Zr phase. Reorientation would then be the result of a change in nucleation sites toward misaligned grains rather than a change in nanoscale hydride shape and orientation.

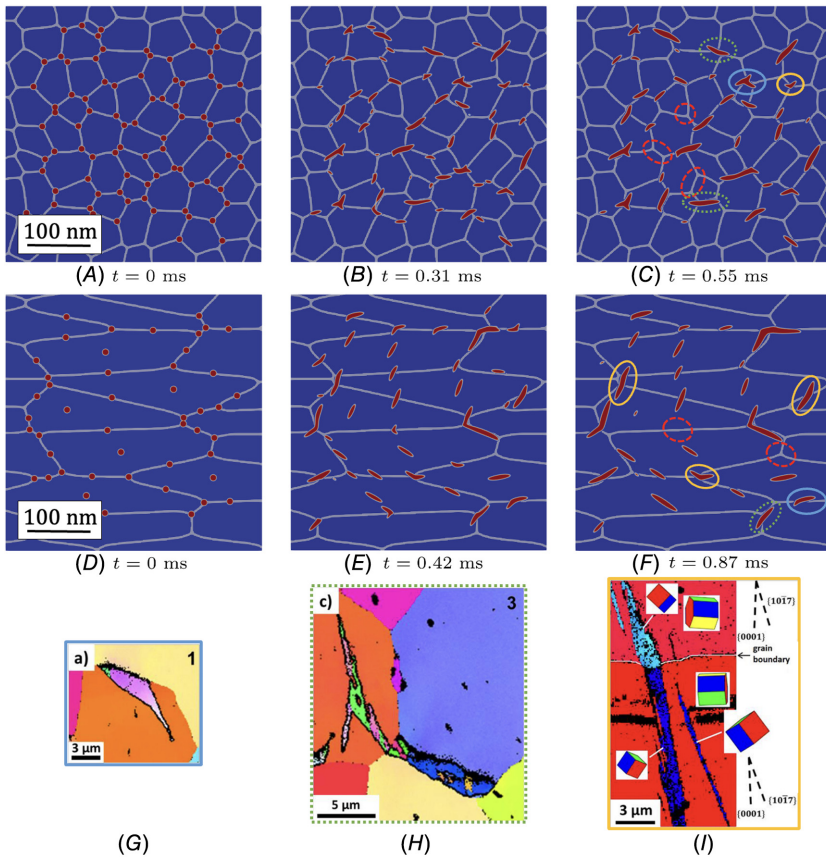
Hydride Precipitation in a Polycrystal

HYDRIDE GROWTH IN ZIRCONIUM POLYCRYSTALS WITHOUT APPLIED STRESS

The growth of hydride particles is simulated in the grain structures shown in **figure 2A** and **C**. In this section, no external load is applied to the simulation domain, and we focus on the interaction between hydrides and grain structure. As discussed earlier, the anisotropy of the polycrystal makes the hydrogen distribution heterogeneous. The heterogeneity of hydrogen distribution and the presence of GBs imply that to accurately simulate hydride nucleation, a heterogeneous nucleation model should be added to the phase-field model. Although such models exist, they are complex and require extensive and accurate knowledge of GB energies, α -Z/ δ -ZrH_{1.66} interfacial energies, and other materials properties that are not yet available. In this work, hydride nuclei are simply added at $t=0$ ms at triple junctions, GBs, and the center of large grains. Hydride particles are free to grow, and coarsening is expected to help hydrides in more favorable positions to grow and make hydrides in less favorable positions dissolve. As such, these simulations focus on the competition between hydrides during growth rather than during nucleation. Simulations were performed with a total hydrogen content of 350 wt.ppm to account for the large number of hydride nuclei.

Figure 5 shows the evolution of hydride morphology in the polycrystals shown in **figure 2A** and **C** and compares predictions against electron backscatter diffraction

FIG. 5 Hydride growth in zirconium polycrystals from [figure 2A](#) and [C](#) in the absence of applied stress and comparison against experimental observations. In (A–F), hydrides are dark and GBs are white/clear. Circular hydrides quickly take on complex shapes to minimize the elastic energy. (G–I) shows experimental images of hydrides in zirconium polycrystal obtained with EBSD.²⁴ In (C) and (F), areas are circled where hydrides have dissolved (dark) or where hydrides resemble what has been observed in (C) (full dark ellipses), (D) (dotted dark ellipses), or (E) (full clear ellipses). The phase-field model captures some aspects of hydride morphology in polycrystals. The domain size is 400×400 nm.



(EBSD) observations published elsewhere.²⁴ It consists of orientation maps of δ hydrides in as-received fine grain and “blocky alpha” large-grain Zircaloy-4. Hydride morphology is quantified across a large section of cladding materials. However, due to the limited number of grains simulated in the current study, we

qualitatively compared our model's predictions with small hydride maps, which show a wide variety of possible hydride morphologies around GBs.

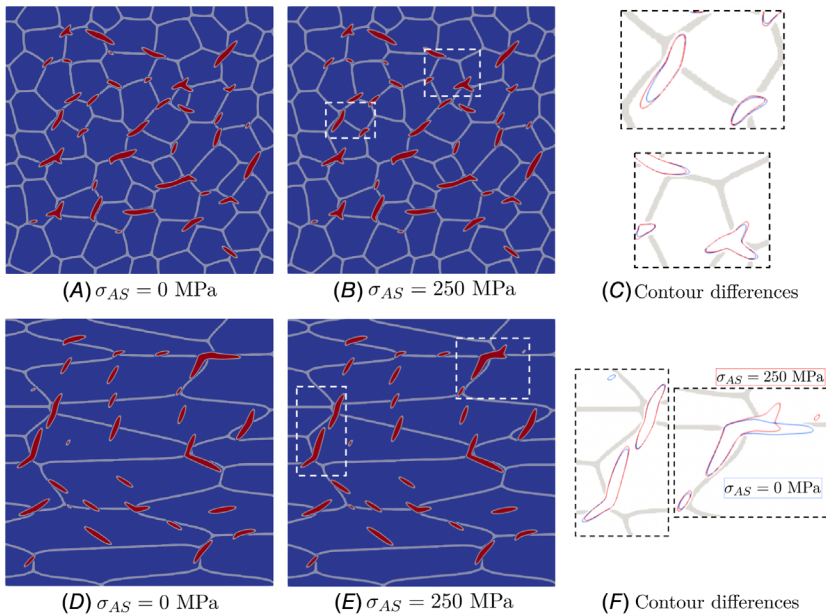
In our simulations, hydrides tend to dissolve in compressed zones, and zones that are more in tension tend to accommodate larger hydride particles. These results suggest that residual stresses and grain texture might affect hydride morphology in polycrystals. Moreover, hydride particles take on a different shape in polycrystals from what is observed in single grains.¹⁷ Although intragranular hydrides still exhibit the ellipsoidal shape, they also exhibit more complex features, becoming S-, V-, L-, or even T-shaped. This is because hydrides sitting in multiple grains simultaneously respect the orientation relationship within each grain and thus grow elongated in different directions depending on the grain orientation. These predictions roughly correspond to the experimental observations shown in [figure 5](#).²⁴ In particular, [figure 5G](#) shows a hydride sitting at a GB with an arm reaching toward the inside of the grain. [Figure 5H](#) shows hydrides sitting at a GB and growing into the grain after reaching the triple junction. Similarly, [figure 5I](#) shows the slight misalignment between two hydrides joined at a GB. Interestingly, these three features are reproduced by the phase-field model, as shown in [figure 5A–F](#).

EFFECT OF APPLIED STRESS ON HYDRIDE GROWTH IN ZIRCONIUM POLYCRYSTALS

The effect of the interaction between grain orientation, hydrides, and applied stress is investigated in the context of the polycrystals shown in [figure 2A](#) and [C](#) to investigate whether stress applied to a polycrystal might promote grain growth in misaligned grains over grains with their basal pole close to the radial direction. Simulations are similar to those presented in [figure 5](#), except that an applied load of 250 MPa has been applied in the circumferential direction (horizontal direction in the figure).

[Figure 6](#) compares the predicted morphologies with and without applied stress. Although the results presented in [figure 6](#) do not show the significant influence of the applied stress on hydride morphology observed experimentally during reorientation, the presence of the applied stress does affect some aspects of hydride morphology. [Figure 6C](#) and [F](#) shows that in both polycrystals, radial hydrides tend to be slightly longer under applied stress, whereas circumferential hydrides are shorter. More notably, [figure 6F](#) shows that one hydride particle reorients by selecting a misaligned grain over an aligned grain under applied stress. Although this hydride grows in a grain with a radially aligned basal pole in the absence of applied stress, it grows in a neighboring misaligned grain under applied load. This reorientation by grain selection is attributed to better stress accommodation by the misaligned grain. Because the *c*-axis of the hcp structure of the α -Zr phase is in tension in the presence of an applied stress, the misaligned grain is better able to accommodate the large stress-free strain along (0001)_z due to the volume/shape misfit between the α -Zr and δ -ZrH_{1.66} phases. Although of a small magnitude, these predictions are consistent with experimental observations showing that, under stress,

FIG. 6 Effect of an applied load of 250 MPa in the circumferential direction on hydride morphology. (A) and (D) show the results without applied stress at $t = 0.55$ ms and $t = 0.87$ ms, respectively, as in [figure 5](#). (B) and (E) show the hydride microstructures under an applied tensile stress of 250 MPa at the same times. Some areas of the domain are highlighted and shown in greater details in (C) and (F). In (C) and (F), the contours of hydrides are shown for the microstructure without and with applied stress. The applied stress influences some aspects of hydride morphology. In particular, (F) shows how one hydride grows circumferentially without applied stress but radially under load, which suggests a path toward reorientation. The domain size is 400×400 nm.



intragranular hydrides tended to preferentially precipitate in the grains with circumferential basal pole textures and in grain faces perpendicular to the direction of the applied stress.⁴⁸

Although in the right direction, these differences between hydride morphology formed with and without applied stress are not significant enough to account for hydride reorientation under applied stress. Running these simulations for a longer time might increase the significance of the effect of the applied stress. The hydride morphologies shown in [figure 6](#) are not at equilibrium, and hydrides are still competing for growth. Some of the limitations of the current calculations are listed below. The results presented here, however, are a first step to quantifying the interaction between the grain structure of the cladding material, the presence of an external load, and hydride morphology.

Discussion

A POTENTIAL MECHANISM FOR HYDRIDE REORIENTATION

Simon et al.¹⁷ suggested that accounting for the polycrystal nature of the cladding material might be necessary to accurately model hydride morphology, especially under applied stress. In the current study we investigated how the zirconium grain structure affects hydrogen distribution and hydride growth, with and without applied stress. We show that adding the polycrystal structure of the zirconium cladding material could provide a path for hydride reorientation.

Simulations of hydrogen diffusion showed that the polycrystal structure of the matrix leads to heterogeneities in hydrogen distribution. The anisotropy of eigenstrains and elastic constants in misoriented grains, as well as the segregation energy at GBs, cause hydrogen atoms to diffuse toward GBs and triple junctions that are in tension. The presence of external applied stress was shown to influence the hydrogen distribution by increasing the concentration in misaligned grains, which could lead to a change in nucleation sites. Although hydrides still grow along the basal plane of their parent grain by nucleating preferentially in misaligned grains, they would grow along the radial direction rather than along the circumferential direction. This mechanism is consistent with previous studies summarized by Ells,⁴⁹ who argued that the nucleation stages determine hydride morphology rather than the growth of stable nuclei.

In this work, we also investigated the role of hydride growth in defining hydride morphology. Simulations of hydride growth were performed in different zirconium polycrystals with different textures, grain shapes, and sizes. Although intragranular hydrides exhibit the same ellipsoidal shape as seen in the single-grain simulations, intergranular hydrides take on more complex shapes when crossing GBs to accommodate the orientation of each grain. These shapes were successfully compared to experimental EBSD observations.²⁴ More importantly, the observed effect of applied load on hydride growth suggests a potential mechanism for hydride reorientation. The presence of a circumferential applied stress has been shown in [figure 6](#) to favor the growth of hydrides in grains with circumferentially aligned basal poles over hydrides in grains with radially aligned basal poles. Radially elongated hydrides thus become longer under applied stress. This prediction is consistent with experimental observations.^{1,8,27,48,49} Using EBSD analysis, Une et al.⁴⁸ experimentally observed that under tensile stress intragranular hydrides tended to preferentially precipitate in the grains with circumferential basal pole textures and intergranular hydrides tended to preferentially precipitate on the grain faces opposite to the tensile axis, as predicted by the current model.

Although the effect of applied stress is minimal in a single grain, it influences both hydrogen distribution and hydride growth in polycrystals. These results indicate a potential mechanism for hydride reorientation. Under applied stress, hydrogen flows to highly misaligned grains and radial GBs because these zones are in tension, thus favoring hydride nucleation. Hydrides then grow in radially oriented

GBs and misaligned grains. Subsequent hydrides nucleate and grow near the tip of existing hydrides to create the stacking structures predicted in Simon et al.¹⁷ However, because hydrides are preferentially in grains misaligned with the direction of the applied stress, the stacking along the basal plane appears radial. This mechanism also explains experimental observations showing that (i) nanoscale hydrides in radial mesoscale hydrides are often highly misaligned with the circumferential direction and (ii) mesoscale hydrides appear either circumferential or radial and do not continuously increase the angle of their habit plane with the magnitude of the applied stress (see [fig. 1](#) and Cinbiz et al.⁸). The threshold stress therefore corresponds to the stress needed to change the location of preferred nucleation sites rather than to a change in nanoscale hydride shape and orientation.

The predicted effect of applied stress on hydrogen distribution and hydride growth, however, does not fully account for the experimentally observed changes in hydride morphology during reorientation. More work and model development are required to verify this hypothesis, and we discuss the limits of the current study in the next section. However, such a model could eventually be used to study the influence of material properties such as alloying elements, texture, and grain shape on hydride morphology with and without applied stress. These insights can drive the development of new materials resistant to hydride reorientation and limit the degree of hydride embrittlement of cladding materials.

LIMITATIONS OF THE CURRENT MODEL AND SUGGESTIONS FOR FUTURE WORK

The current phase-field model is limited in time and in size. Performing these simulations on a larger time scale could influence the results and increase the role of applied stress in determining hydride morphology. It would also allow simulating thermomechanical cycles, which have been shown to promote hydride reorientation. Currently, the model is limited to simulating the equivalent of a short quench at 550 K, where the hydrogen quickly precipitates into hydrides. Experimentally, these thermal treatments do not promote hydride reorientation. Slower, repeated cooling processes do.^{1,8,10,11} Quick hydride precipitation is expected to be mainly governed by the minimization of chemical energy and internal stresses, whereas slow precipitation emphasizes the importance of external stresses and growth. The fact that the current model can predict a slight reorientation during a short quench suggests that performing the same simulation during a longer timescale would result in a significant increase in hydride reorientation.

The computational limit on the size of the simulations prevents the simulation of the full mesoscale hydride morphology and limits a one-to-one comparison with experimental observations. In particular, the average grain size of the microstructures simulated in this study (50 nm) are significantly smaller than the 1- μm experimentally observed grain sizes. However, as discussed earlier and measured in Kearns and Woods,²⁷ modeling many small grains provides more opportunities for grain selection than a few large grains. Simulating hydride precipitation in 3D

domains is also expected to influence the model's predictions. Simon et al.¹⁷ showed that hydride morphology can only be accurately simulated in 3D domains. Even if the current study has favored the domain size and the number of grains over the number of dimensions of the domain, future work should focus on performing these simulations in 3D to improve the accuracy of the predictions.

The absence of plasticity in the calculation and the lack of available data on the properties of the α -Zr/ δ -ZrH_{1.66} interface were discussed in Simon et al.¹⁷ but are not expected to significantly affect the mechanism of grain selection investigated in this study. Moreover, introducing the zirconium grain structure required additional assumptions about material properties such as the GB energies. For example, the segregation energy introduced in the current model is assumed to be isotropic, whereas it likely varies from GB to GB. Given the crucial role of GBs in hydride morphology already exhibited in the current work, a more accurate description of the GBs could improve the model's prediction. In the current model, the elastic properties of the GBs are interpolated between the neighboring grains, as explained earlier. However, in real materials, the GB is expected to accommodate some of the strains. Experimentally, hydrides have been observed to grow along the GBs.^{24,48} However, in the current model, hydrides grow along the GB only when it is parallel to the basal plane of one of the parent grains. Introducing some relaxation of the eigenstrains of the system at the GBs might promote hydrogen precipitation at GBs and influence the overall hydride morphology. Unfortunately, to our knowledge, no data are available on the degree to which GBs might accommodate hydrides better than grains. Despite these limitations, the current work represents a significant improvement in the understanding of the role of the zirconium grain structure in governing hydride morphology.

Conclusion

In this study, we investigated hydrogen distribution and hydride precipitation in polycrystalline zirconium. A previous phase-field model focused on hydride precipitation in a single zirconium crystal showed that although circumferential hydride stacking under no applied stress was predicted, radial stacking (i.e., hydride reorientation) was unlikely under reasonable applied stress. In this study, we therefore expanded that model to account for the polycrystalline structure of the zirconium matrix to explore other mechanisms for hydride reorientation. Even without applied stress, we showed that the polycrystalline structure influences hydrogen distribution and hydride morphology, as misoriented grains with anisotropic elastic properties and thermal strains interact and create a heterogeneous strain field. The predicted hydride morphology roughly corresponds to features of experimental observations.

Moreover, grains with different orientations react differently to an applied stress. Under a circumferentially applied stress, grains with a circumferentially aligned basal pole better accommodate hydrogen atoms and hydrides. The presence

of applied stress thus influences the type of preferred grains. Nanoscale hydrides thus tend to grow in misaligned grains. Although still elongated along the basal planes of the zirconium matrix, they appear radial due to the grains' misalignment. This mechanism leads to radial hydride stacking. As a result, whereas simulations of hydride precipitation in a single grain failed to predict hydride reorientation under reasonable applied stress, the polycrystal structure allows for new mechanisms to occur. Due to the model's limitations (e.g., time and space limitations), this effect is still limited in the current work. However, this constitutes an important step in recognizing the potential role of the grain structure in hydride reorientation, and suggested improvements and experiments can further extend the newly proposed mechanism for hydride reorientation.

ACKNOWLEDGMENTS

This work was performed with the support of the U.S. Department of Energy NEUP IRP-17-13708 project "Development of a Mechanistic Hydride Behavior Model for Spent Fuel Cladding Storage and Transportation." This research made use of the resources of the High Performance Computing Center at Idaho National Laboratory, which is supported by the Office of Nuclear Energy of the U.S. Department of Energy and the Nuclear Science User Facilities under Contract No. DE-AC07-05ID14517.

References

1. A. T. Motta, L. Capolungo, L.-Q. Chen, M. N. Cinbiz, M. R. Daymond, D. A. Koss, E. Lacroix et al., "Hydrogen in Zirconium Alloys: A Review," *Journal of Nuclear Materials* 518 (2019): 440–460.
2. F. Passelaigue, P.-C. A. Simon, and A. T. Motta, "Predicting the Hydride Rim by Improving the Solubility Limits in the Hydride Nucleation-Growth-Dissolution (HNGD) Model," *Journal of Nuclear Materials* 558 (2022): 153363.
3. E. Lacroix, "Modeling Zirconium Hydride Precipitation and Dissolution in Zirconium Alloys" (PhD thesis, Pennsylvania State University, 2019).
4. E. Lacroix, A. T. Motta, and J. D. Almer, "Experimental Determination of Zirconium Hydride Precipitation and Dissolution in Zirconium Alloy," *Journal of Nuclear Materials* 509 (2018): 162–167.
5. F. Passelaigue, E. Lacroix, G. Pastore, and A. T. Motta, "Implementation and Validation of the Hydride Nucleation-Growth-Dissolution (HNGD) Model in BISON," *Journal of Nuclear Materials* 544 (2021): 152683.
6. E. Lacroix, P.-C. A. Simon, A. T. Motta, and J. Almer, "Zirconium Hydride Precipitation and Dissolution Kinetics in Zirconium Alloys," in *Zirconium in the Nuclear Industry: 19th International Symposium*, ed. A. T. Motta and S. K. Yagnik (West Conshohocken, PA: ASTM International, 2021), STP 1622. 67–91 <https://doi.org/10.1520/STP162220190035>
7. P.-C. A. Simon, C. Frank, L.-Q. Chen, M. R. Daymond, M. R. Tonks, A. T. Motta, "Quantifying the Effect of Hydride Microstructure on Zirconium Alloys Embrittlement Using Image Analysis," *Journal of Nuclear Materials* 547 (2021): 152817.
8. M. N. Cinbiz, D. A. Koss, A. T. Motta, J. S. Park, and J. D. Almer, "In Situ Synchrotron X-Ray Diffraction Study of Hydrides in Zircaloy-4 during Thermomechanical Cycling," *Journal of Nuclear Materials* 487 (2017): 247–259.

9. K. Colas, A. T. Motta, M. R. Daymond, and J. Almer, "Mechanisms of Hydride Reorientation in Zircaloy-4 Studied In Situ," in *Zirconium in the Nuclear Industry: 17th Volume*, ed. R. J. Comstock and P. Barberis (West Conshohocken, PA: ASTM International, 2015), STP 1543, 1107–1137, <https://doi.org/10.1520/STP154320120168>
10. K. B. Colas, A. T. Motta, M. R. Daymond, and J. D. Almer, "Effect of Thermo-Mechanical Cycling on Zirconium Hydride Reorientation Studied In Situ with Synchrotron X-Ray Diffraction," *Journal of Nuclear Materials* 440 (2013): 586–595.
11. K. B. Colas, A. T. Motta, J. D. Almer, M. R. Daymond, M. Kerr, A. D. Banchik, P. Vizcaino, and J. R. Santisteban, "In Situ Study of Hydride Precipitation Kinetics and Re-Orientation in Zircaloy Using Synchrotron Radiation," *Acta Materialia* 58 (2010): 6575–6583.
12. M. N. Cinbiz, D. A. Koss, and A. T. Motta, "The Influence of Stress State on the Reorientation of Hydrides in a Zirconium Alloy," *Journal of Nuclear Materials* 477 (2016): 157–164.
13. L.-Q. Chen, "Phase-Field Models for Microstructure Evolution," *Annual Review of Materials Research* 32 (2003): 113–140.
14. N. Moelans, B. Blanpain, and P. Wollants, "An Introduction to Phase-Field Modeling of Microstructure Evolution," *Calphad* 32 (2008): 268–294.
15. A. T. Motta and L.-Q. Chen, "Hydride Formation in Zirconium Alloys," *JOM* 64 (2012): 1403–1408.
16. J. Bair, M. Asle Zaeem, and M. R. Tonks, "A Review on Hydride Precipitation in Zirconium Alloys," *Journal of Nuclear Materials* 466 (2015): 12–20.
17. P.-C. A. Simon, L. K. Aagesen, A. M. Jokisaari, L. Q. Chen, M. R. Daymond, A. T. Motta, and M. R. Tonks, "Investigation of δ Zirconium Hydride Morphology in a Single Crystal Using Quantitative Phase Field Simulations Supported by Experiments," *Journal of Nuclear Materials* 557 (2021): 153303.
18. A. M. Jokisaari and K. Thornton, "General Method for Incorporating CALPHAD Free Energies of Mixing into Phase Field Models: Application to the α -Zirconium/ δ -Hydride System," *Calphad* 51 (2015): 334–343.
19. J. Bair, M. Asle Zaeem, and D. Schwen, "Formation Path of δ Hydrides in Zirconium by Multiphase Field Modeling," *Acta Materialia* 123 (2017): 235–244.
20. A. Toghraee, J. Bair, and M. Asle Zaeem, "Effects of Applied Load on Formation and Reorientation of Zirconium Hydrides: A Multiphase Field Modeling Study," *Computational Materials Science* 192 (2021): 110367.
21. T. W. Heo, K. B. Colas, A. T. Motta, and L.-Q. Chen, "A Phase-Field Model for Hydride Formation in Polycrystalline Metals: Application to δ -Hydride in Zirconium Alloys," *Acta Materialia* 181 (2019): 262–277.
22. G. M. Han, Y. F. Zhao, C. B. Zhou, D.-Y. Lin, X. Y. Zhu, J. Zhang, S. Y. Hu, and H. F. Song, "Phase-Field Modeling of Stacking Structure Formation and Transition of δ -Hydride Precipitates in Zirconium," *Acta Materialia* 165 (2019): 528–546.
23. B. Radhakrishnan, S. B. Gorti, K. Clarno, and Y. Yan, "Phase Field Simulations of Hydride Reorientation in Zircaloys" (paper presentation, International High-Level Radioactive Waste Management Conference, Albuquerque, NM, April 28–May 2, 2013).
24. S. Wang, F. Giuliani, and T. B. Britton, "Microstructure and Formation Mechanisms of δ -Hydrides in Variable Grain Size Zircaloy-4 Studied by Electron Backscatter Diffraction," *Acta Materialia* 169 (2019): 76–87.
25. M. A. Louchez, L. Thuinet, R. Besson, and A. Legris, "Microscopic Phase-Field Modeling of hcp|fcc Interfaces," *Computational Materials Science* 132 (2017): 62–73.
26. Y. Zhang, X.-M. Bai, J. Yu, M. R. Tonks, M. J. Noordhoek, and S. R. Phillpot, "Homogeneous Hydride Formation Path in α -Zr: Molecular Dynamics Simulations with the Charge-Optimized Many-Body Potential," *Acta Materialia* 111 (2016): 357–365.

27. J. J. Kearns and C. R. Woods, "Effect of Texture, Grain Size, and Cold Work on the Precipitation of Oriented Hydrides in Zircaloy Tubing and Plate," *Journal of Nuclear Materials* 20 (1966): 241–261.
28. *Grain Size Determination in Zirconium Alloys*, IAEA-TECDOC-794 (Vienna, Austria: International Atomic Energy Agency, 1995).
29. J. A. Szpunar, W. Qin, H. Li, and N. A. P. Kiran Kumar, "Roles of Texture in Controlling Oxidation, Hydrogen Ingress and Hydride Formation in Zr Alloys," *Journal of Nuclear Materials* 427 (2012): 343–349.
30. S. G. Kim, W. T. Kim, and T. Suzuki, "Phase-Field Model for Binary Alloys," *Physical Review E* 60 (1999): 7186, <https://doi.org/10.1103/PhysRevE.60.7186>
31. L. K. Aagesen, D. Schwen, K. Ahmed, and M. R. Tonks, "Quantifying Elastic Energy Effects on Interfacial Energy in the Kim-Kim-Suzuki Phase-Field Model with Different Interpolation Schemes," *Computational Materials Science* 140 (2017): 10–21.
32. P.-C. A. Simon, L. K. Aagesen, A. T. Motta, and M. R. Tonks, "The Effects of Introducing Elasticity Using Different Interpolation Schemes to the Grand Potential Phase Field Model," *Computational Materials Science* 183 (2020): 109790.
33. N. Moelans, "A Quantitative and Thermodynamically Consistent Phase-Field Interpolation Function for Multi-Phase Systems," *Acta Materialia* 59 (2011): 1077–1086.
34. A. G. Khachaturyan, *Theory of Structural Transformations in Solids* (New York, NY: Dover Publications, 2008).
35. G. J. C. Carpenter, "The Dilatational Misfit of Zirconium Hydrides Precipitated in Zirconium," *Journal of Nuclear Materials* 48 (1973): 264–266.
36. S. R. MacEwen, C. E. Coleman, C. E. Ells, and J. Faber, "Dilation of h.c.p. Zirconium by Interstitial Deuterium," *Acta Metallurgica* 33 (1985): 753–757.
37. G. B. Skinner and H. L. Johnston, "Thermal Expansion of Zirconium between 298 °K and 1600 °K," *Journal of Chemical Physics* 21 (1953): 1383–1384.
38. M. N. Cinbiz, X. Hu, and K. Terrani, "Thermal Expansion Behavior of δ -Zirconium Hydrides: Comparison of δ Hydride Powder and Platelets," *Journal of Nuclear Materials* 509 (2018): 566–576.
39. C. J. Permann, M. R. Tonks, B. Fromm, and D. R. Gaston, "Order Parameter Re-Mapping Algorithm for 3D Phase Field Model of Grain Growth Using FEM," *Computational Materials Science* 115 (2016): 18–25.
40. P.-C. A. Simon, "Phase Field Modeling and Quantification of Zirconium Hydride Morphology" (PhD diss., Pennsylvania State University, 2021).
41. P.-C. A. Simon, L. K. Aagesen, C. Jiang, W. Jiang, and J.-H. Ke, "Mechanistic Calculation of the Effective Silver Diffusion Coefficient in Polycrystalline Silicon Carbide: Application to Silver Release in AGR-1 TRISO particles," *Journal of Nuclear Materials* 563 (2022): 153669.
42. P.-C. A. Simon, L. Aagesen, C. Jiang, W. Jiang, and J.-H. Ke, "Jupyter Script for Automatic Polycrystalline Generation with Desired Grain Size and Elongation," *Mendeley Data* 1 (2021): <https://doi.org/10.17632/VH78XY85F1>
43. M. Christensen, T. M. Angelii, J. D. Ballard, J. Vollmer, R. Najafabadi, and E. Wimmer, "Effect of Impurity and Alloying Elements on Zr Grain Boundary Strength from First-Principles Computations," *Journal of Nuclear Materials* 404 (2010): 121–127.
44. C. J. Permann, D. R. Gaston, D. Andrš, R. W. Carlsen, F. Kong, A. D. Lindsay, J. M. Miller et al., "MOOSE: Enabling Massively Parallel Multiphysics Simulation," *SoftwareX* 11 (2020): 100430.
45. D. Gaston, C. Newman, G. Hansen, and D. Lebrun-Grandié, "MOOSE: A Parallel Computational Framework for Coupled Systems of Nonlinear Equations," *Nuclear Engineering and Design* 239 (2009): 1768–1778.

46. M. R. Tonks, D. Gaston, P. C. Millett, D. Andrs, and P. Talbot, "An Object-Oriented Finite Element Framework for Multiphysics Phase Field Simulations," *Computational Materials Science* 51 (2012): 20–29.
47. D. Schwen, L. K. Aagesen, J. W. Peterson, and M. R. Tonks, "Rapid Multiphase-Field Model Development Using a Modular Free Energy Based Approach with Automatic Differentiation in MOOSE/MARMOT," *Computational Materials Science* 132 (2017): 36–45.
48. K. Une, K. Nogita, S. Ishimoto, and K. Ogata, "Crystallography of Zirconium Hydrides in Recrystallized Zircaloy-2 Fuel Cladding by Electron Backscatter Diffraction," *Journal of Nuclear Science and Technology* 41 (2004): 731–740.
49. C. E. Ells, "The Stress Orientation of Hydride in Zirconium Alloys," *Journal of Nuclear Materials* 35 (1970): 306–315.

Discussion

Question from Brendan Ensor, Naval Nuclear Laboratory:—Have you examined different applied stress levels (higher or lower) to see whether the degree of hydride reorientation would change as a function of stress?

Authors' Response:—The only stress levels that we investigated in this study were no applied stress and 250 MPa of tensile stress in the hoop direction. The goal of the current study is to investigate mechanisms that could be responsible for hydride reorientation at the mesoscale under a reasonable applied stress. By introducing the polycrystalline structure of the zirconium matrix, we show that grain selection under reasonable applied stress could lead to hydride reorientation. However, although we predict reorientation under applied stress and a higher applied stress would be expected to lead to greater grain selection, the computational costs of the model would need to be decreased to allow a quantitative study of the link between stress level and degree of reorientation.

Question from Philipp Frankel, University of Manchester:—Do the contours of hydrides shown from the model represent individual hydrides or hydride platelets? Do you allow changes in orientation relationships as hydrides reorient?

Authors' Response:—The contours of the hydrides in this study show nanoscale hydrides—not mesoscale hydride platelets. However, as shown in [figure 5F](#) and [1](#), modeled hydrides do change direction as they cross GBs and enter different grains. In that case, they represent two or three different hydride particles joining at a GB or triple junction. On each side of the GB or triple junction, the phase-field calculation predicts that the nanoscale hydride particle respects the original orientation relationship with that grain.

We therefore do not predict any orientation relationship change as hydrides reorient. This mechanism has been explored by other studies, but it requires an unreasonably high applied stress. Rather, the current mechanism predicts that the hydride particles respect the orientation relationship but nucleate and grow in different grains with basal poles aligned with the direction of the applied stress.

This grain-selection mechanism for hydride reorientation is shown to be possible under an applied stress of 250 MPa. More details are available in the section “Effect of Applied Stress on Hydride Growth in Zirconium Polycrystals.”

Question from Adrien Couet, University of Wisconsin–Madison:—Have you tried to come up with a more quantitative factor for the hydride reorientation under stress to determine whether indeed hydrides reorient? What is the actual time of a simulation?

Authors’ Response:—The actual time of the simulations are provided in the captions of the relevant figures and are up to 1 ms. This is an important limitation of the current modeling approach, as discussed in detail in the paper. For that reason, it would be challenging to come up with a quantitative factor for hydride reorientation that would be relevant for engineering applications. However, the goal of the current study was to investigate mechanisms that could be responsible for hydride reorientation at the mesoscale under a reasonable applied stress, and introducing the polycrystalline structure of the zirconium matrix did show that grain selection could lead to hydride reorientation, as shown in [figure 6F](#) and discussed in the paper. Both hydrogen diffusion toward misaligned grains and hydride preferential growth in misaligned grains were predicted by the model and would contribute to hydride reorientation.

Question from Sara Weick, KIT:—Did you include or have you thought about the hydride orientation scenarios in the presence of second-phase particles?

Authors’ Response:—Unfortunately, no. The current study focuses on the effect of the polycrystalline zirconium structure and applied stress on hydrogen distribution and hydride morphology. To limit computational costs, but also to isolate the desired mechanisms, we use a simplified version of the microstructure that does not include every aspect of the real microstructure and microchemistry. The role of second-phase particles has therefore not been investigated.

Question from Michael Preuss, Monash University and University of Manchester:—How did you determine your thermal anisotropic strains considering they are notoriously difficult to determine? And do you not think that uncertainty here means that your model is mainly about showing mechanisms but absolute/critical values cannot be obtained from it? Just to add that the mechanism you are showing here is already a great contribution.

Authors’ Response:—The anisotropic thermal eigenstrains were obtained from Skinner and Johnston¹ and Cinbiz et al.,² which are assumed to be valid for isothermal precipitation at $T = 550$ K, without accounting for relaxation or viscoplastic effects. As for many other values used in the current model, either experimentally

measured or derived from lower length scale calculations, significant uncertainties are expected. We nevertheless used these values to develop a quantitative model and show that the proposed hydride reorientation mechanism is possible at reasonable stress levels. However, as you rightly point out, these uncertainties must be considered when deriving absolute/critical values from the current model. It would therefore be premature to extract from the current model a quantitative link between the magnitude of the applied stress and the degree of hydride reorientation. A careful sensitivity analysis must first be performed to understand and quantify uncertainty propagation.

1. G. B. Skinner and H. L. Johnston, "Thermal Expansion of Zirconium between 298 °K and 1600 °K," *Journal of Chemical Physics* 21 (1953): 1383–1384.
2. M. N. Cinbiz, X. Hu, and K. Terrani, "Thermal Expansion Behavior of δ -Zirconium Hydrides: Comparison of δ Hydride Powder and Platelets," *Journal of Nuclear Materials* 509 (2018): 566–576.